

Laser isotope separation of uranium

P. Ramakoteswara Rao

7 Saras Baug, Deonar, Mumbai 400 088, India

A research effort was carried out at the Bhabha Atomic Research Centre (BARC), Mumbai, for developing laser-based techniques for enrichment of natural uranium to reactor-grade (2.5% to 3.0% ^{235}U), with the potential to be economically scalable to industrial production. Three approaches – two molecular, namely CO_2 laser-based approach and UF_6 -based approach, and one atomic, namely Atomic Vapour Laser Isotope Separation (AVLIS) – were investigated. The AVLIS method was found to be the best, and was pursued to achieve the goal. In the AVLIS technique, uranium atomic vapour was isotope selectively ionized by three copper vapour laser pumped pulsed dye lasers, and the ions were collected by an electric field. This method could enrich uranium to several times the targetted figure. It is scalable, though some difficult technological problems have to be addressed. The basic scientific aspects of the three approaches and details of the AVLIS technique are presented in this paper.

THE need for enriched uranium for light water-moderated power reactors, breeder reactors and other uses is well known. Till recently, all enriched uranium was produced essentially by two techniques – gaseous diffusion and centrifugation. Presently, enrichment by laser techniques has the promise to become commercially competitive, and is in various stages of development in a few technically advanced countries.

With the advent of continuously tunable lasers on the scientific scene in the early 1970s, several scientists around the globe, including the author of this article were of the view that tunable lasers could be used for isotope separation, in particular for uranium enrichment. The present author made a formal proposal for initiating research in the relevant areas of spectroscopy, photochemistry and laser development converging towards development of a method for enrichment of uranium, which was approved. A new research activity under the Multi-disciplinary Research Scheme (MDRS) was initiated.

Many elements in the periodic table have two or more naturally occurring isotopes; for example, uranium has three isotopes with abundances as shown in parentheses – ^{238}U (99.3%), ^{235}U (0.7%) and ^{234}U (0.054%). Each spectral line of any element exhibits as many components as the number of isotopes, slightly shifted in wavelength from one another. These spectral shifts are known as isotope

shifts, which are usually small and often unresolved. Similarly, spectral lines of molecules also exhibit isotope shifts, contributed by one or more component atoms.

Isotope shift in the uranium atomic line at 436.2 nm, recorded in our laboratory, is shown in Figure 1 and, that in the Q-branch of the ν_3 band at 625.5 cm^{-1} of a molecular beam of UF_6 supercooled to $\approx 30\text{ K}$ is shown in Figure 2 (see ref. 1). It may be noted that the isotopic features are resolved from each other with hardly any overlap in both the pictures, an essential requirement for laser isotope separation (LIS). Since fluorine has a single isotope, isotopic shifts in UF_6 molecule are solely due to uranium isotopes.

The basic principle of LIS is shown in Figure 3. Isotopic selective excitation of an atom or molecule using a tunable laser is followed by ionization of the selectively excited atom or dissociation of the selectively excited

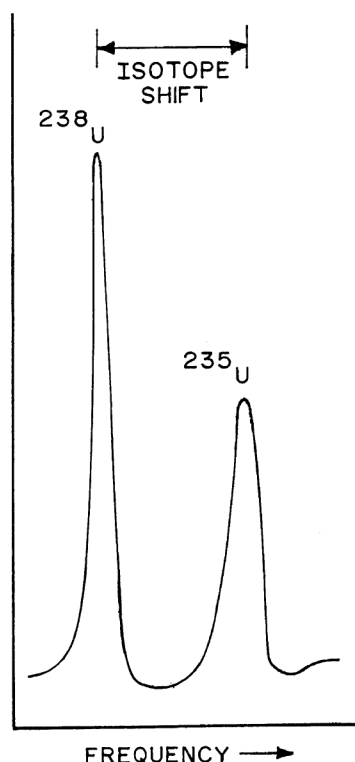


Figure 1. Isotope structure of the 436.2 nm line of uranium from a liquid nitrogen-cooled U-hollow cathode lamp, recorded in our laboratory with a Recording Fabry–Perot Spectrometer. The sample used had 47.1% of ^{235}U . The larger width of the ^{235}U component is due to its hyperfine structure. The isotope shift is 415.73 milli-Kaisers.

molecule by another laser. Due to the high monochromaticity of the laser, the other isotopes are not involved in the excitation process, and due to high laser intensities, all or most of the desired isotopic atoms or molecules are excited and ionized/dissociated².

The excitation process can be carried out in one or more steps. Retaining as much of the selectivity achieved in the excitation step(s) as possible till the atoms/molecules are ionized/dissociated and physically separated out of the laser interaction zone, is important for the efficiency of LIS process. A large fraction of the atoms will be in the ground state at the operating temperature. If the ground state has no hyperfine structure, like for ^{238}U , a single-mode tunable dye laser will involve most of the atoms in the

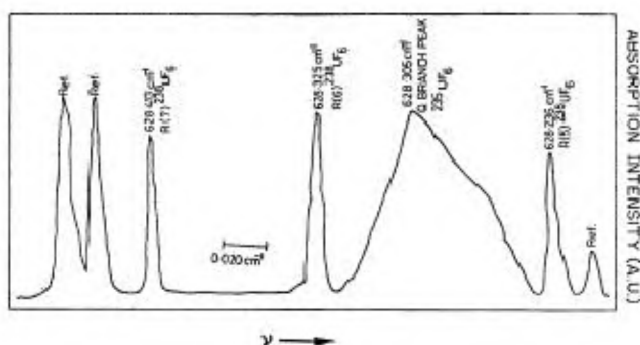


Figure 2. High-resolution IR spectrum of UF_6 supercooled to 30 K in a nozzle beam set-up, recorded with a diode laser spectrometer. R(5), R(6) and R(7) are the R-branch lines of the $0-\nu_3$ band. The Q-branch shows only an envelope of unresolved Q-branch lines.

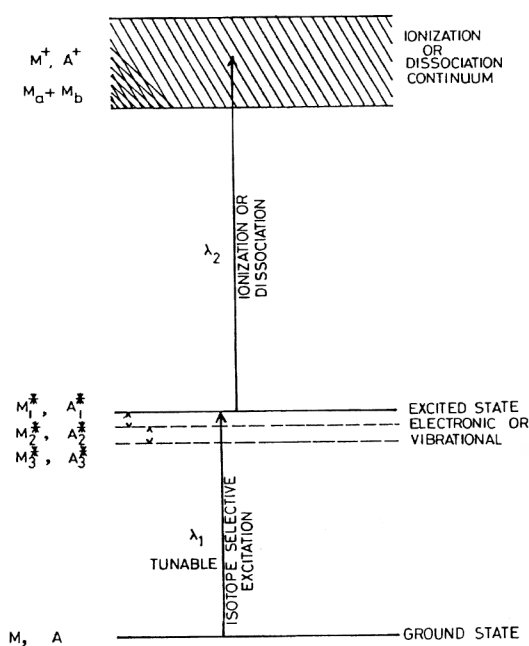


Figure 3. Basic principle of LIS. A_1, A_2, A_3 are three isotopes of atom A . Similarly, M_1, M_2, M_3 are three isotopic species of molecule M , and M_a and M_b are its dissociation products.

ground state in the excitation process. If the ground state has hyperfine structure, as in the case of ^{235}U , a tunable laser with a few closely-spaced axial modes or a frequency-chirped single-mode laser will be needed. In the case of molecules, specially like UF_6 , with small vibrational frequencies and rotational intervals, the molecules are distributed over several vibrational and hundreds of rotational energy levels at room temperature. A single excitation laser can address only a small fraction of the available molecules and, consequently, the basic process becomes inefficient. In order to involve most of the molecules in the excitation process, the molecular vapour has to be super-cooled to low temperatures so that most of the molecules are in the lower rotational levels of the lowest vibrational level. This will also result in almost non-overlapping absorption features of the isotopic molecules, ideal for isotope selective excitation, as seen in Figure 2. The electronic and vibrational-rotational absorption spectra of complex uranium-bearing molecules are too complicated to have non-overlapping uranium isotopic absorption features. Besides, there is additional complication due to isotope shifts of other atoms. Hence, one has to look for minor differences in the relative absorption cross-sections of the two uranium isotopic molecules in the IR absorption spectrum.

LIS of sulphur

To get a feel for LIS experiments, we started by first separating sulphur isotopes of masses 32 and 34 by multiphoton dissociation of SF_6 (ref. 3) using a transversely excited atmospheric (TEA) CO_2 laser built in the Laser Division at BARC (Figure 4). Some CO_2 laser lines overlap the Q-branch of the ν_3 band of SF_6 ($920-960\text{ cm}^{-1}$).

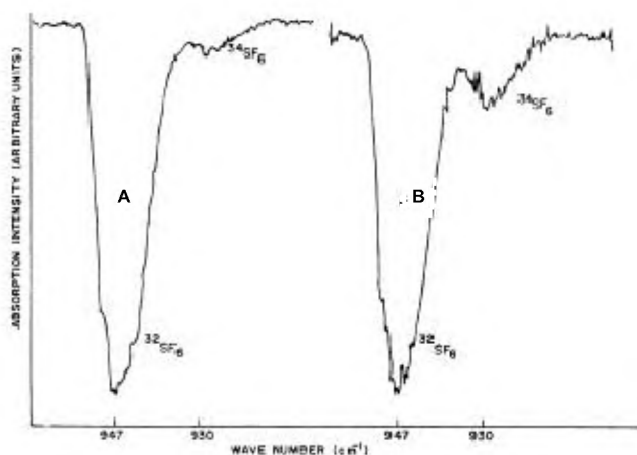


Figure 4. LIS of sulphur isotopes. Curve A, IR absorption spectrum of SF_6 in a 12-cm cell at room temperature (vapour pressure 0.17 torr). Curve B, IR absorption spectrum after irradiation with 1900 TEA CO_2 laser pulses, 1 J/pulse. Over 60% of $^{32}\text{SF}_6$ was dissociated with no dissociation of $^{34}\text{SF}_6$. SF_6 got enriched in ^{34}S from 4.2 to 11.7%.

LIS of uranium

As mentioned earlier, there are two basic approaches, with some sub-approaches for LIS. The strategy adopted was to initiate research work in all the approaches, and quickly build adequate research infrastructure. We were to periodically review these approaches, based on our experimental results as well as by monitoring trends from a few laboratories abroad working on this problem, and take a decision at an appropriate time to concentrate on the most promising approach, and phase-off the others.

Molecular laser isotope separation

Molecular Laser Isotope Separation (MLIS) has two sub-approaches – CO₂ laser-based approach and UF₆ molecule-based approach.

CO₂ laser-based approach

The basic motivation for pursuing this approach was to take advantage of the high-power CO₂ laser technology developed for other applications, like metal cutting and welding. The first scientific challenge here was to synthesize a uranium-bearing compound having absorption features in the region 9.5–10.5 μm , where CO₂ lases on several lines. After going through the relevant literature, two candidate molecules were identified – uranium tetraborohydride, [U(BH)₄]₄, and bis (1,1,1,5,5,5-hexafluoropentane-2,4 dinato) dioxo-uranium (VI) tetrahydrofuran, UO₂[(CF₃CO)₂CH]₂.THF. (These compounds were prepared in the then Chemistry Division at BARC). The latter was chosen for detailed studies. The structure of the molecule⁴ and its IR absorp-

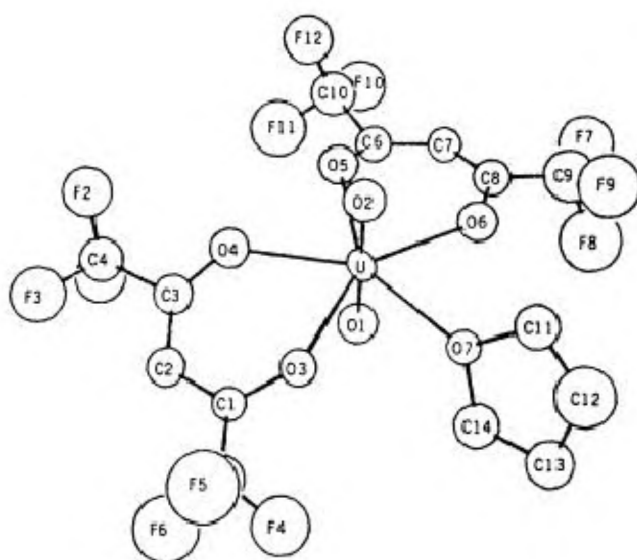


Figure 5. Structure of UO₂[(CF₃CO)₂CH]₂.THF. Labels refer to the atomic constituents of the molecule.

tion spectrum in relation to the frequencies of CO₂ laser lines⁵ are shown in Figures 5 and 6, respectively.

A molecular beam set-up with heating arrangement was made and used for studying photodissociation of the molecule with an on-line quadrupole mass spectrometer (QMS), as shown schematically in Figure 7. The molecular beam was illuminated with the 10P(6) line of the grating-tuned Lumonics 103-2 TEA CO₂ laser, pulse repetition rate 0.5 Hz, and pulse energy 85 mJ/cm². The main mass spectral peak of UO₂[(CF₃CO)₂CH]₂.THF is UO₂(CF₃CO)₂CH.THF⁺ ($m = 549$ a.u. for ²³⁸U-bearing species). The mass spectral peaks at 549 and 546 (for the ²³⁵U-bearing species) were monitored on-line as the laser photolysed the molecular beam (Figure 8). It is seen that there is 30% decomposition of ²³⁸U-bearing molecules against only 5% of ²³⁵U-bearing molecules, which showed that the dissociation fragment was enriched in ²³⁸U by an enrichment factor of 3.4, and the undissociated original molecule was enriched in ²³⁵U by a factor of 1.3. Similar experiments in a closed cell did not show any isotopic selectivity.

This experiment was successful in demonstrating uranium isotope-selective dissociation of a complex molecule with a TEA CO₂ laser. This activity was phased out after concluding that it was unlikely to be competitive vis-à-vis the molecular approach based on UF₆ and the atomic approach. But in the process, preparation of complex organometallic compounds of uranium, setting up of a molecular beam apparatus for studying laser photolysis of compounds using an on-line quadrupole mass spectrometer, i.e. the basic scientific infrastructure for carrying out such experiments was created.

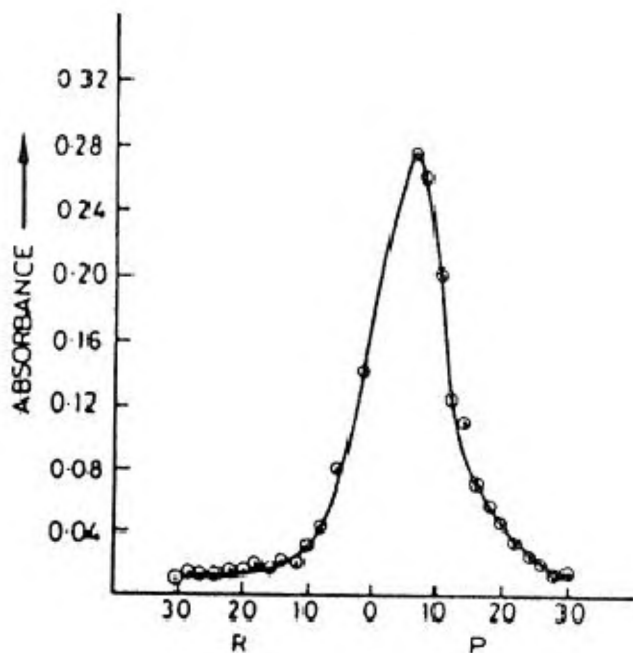


Figure 6. Absorption spectrum of UO₂[(CF₃CO)₂CH]₂.THF as a function of CO₂ laser frequencies. Positions of P and R-lines of the 10.6 μm lasing transition of CO₂ molecule are shown.

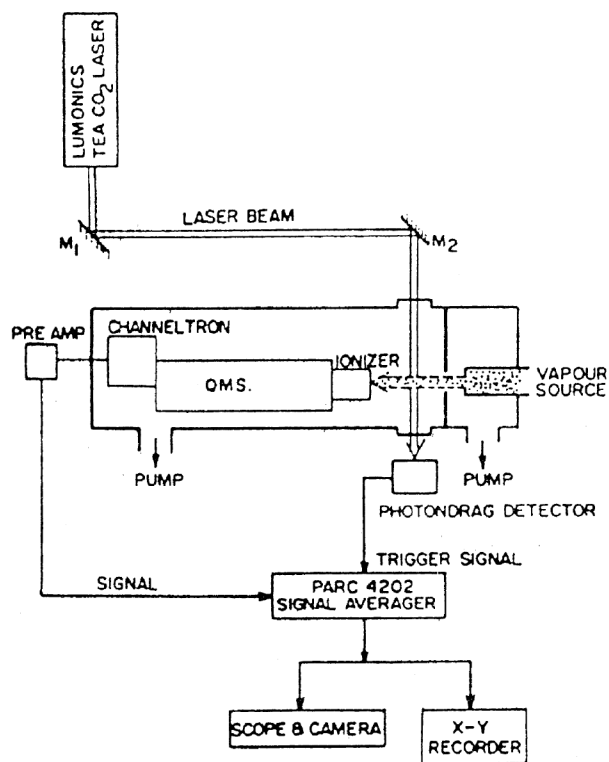


Figure 7. Schematic of the experimental arrangement for on-line studies of photodissociation of volatile compounds.

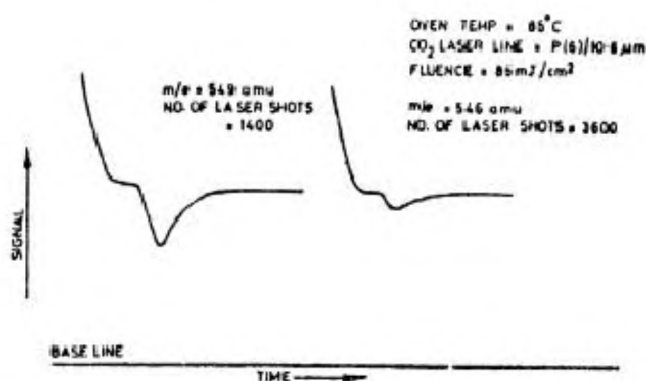


Figure 8. Signal averager output for ions of mass 549 amu (^{238}U fragment) and 546 amu (^{235}U fragment).

UF₆ molecule-based approach

The rationale of this approach was to take advantage of the fact that UF₆ had been produced and handled on an industrial scale, and a large amount of scientific and engineering data on UF₆ were available. The main scientific problems in this approach were: (i) supercooling of UF₆ to around 30 K, (ii) exactly locating the Q-branch head structure of the ν_3 bands of $^{238}\text{UF}_6$ and $^{235}\text{UF}_6$, and (iii) building a laser with its lasing features exactly coinciding with the Q-branch head of the supercooled $^{235}\text{UF}_6$. The laser should be potentially scalable to kilowatts of power.

The difficult engineering problems are to supercool huge amounts of UF₆ and build 16 micron lasers operating for long durations at kilowatts of power.

Two research programmes were initiated – to set-up a facility for supercooling molecular vapours and study their high resolution IR spectra and, simultaneously to develop a suitable IR laser for isotope-selective excitation/dissociation of supercooled UF₆.

Among the six fundamental vibrations of UF₆, ν_1 to ν_6 , only ν_3 at 625.5 cm^{-1} and ν_4 at 186.2 cm^{-1} are IR-active (absorbing) vibrations, which can be used for selective excitation. Of these, ν_3 is a better choice because of its larger isotope shift (0.65 cm^{-1}) and more convenient frequency location. A theoretical and experimental programme was initiated to investigate some basic aspects of laser photochemistry of UF₆ using a TEA CO₂ laser.

The infrared multiphoton dissociation (IRMPD) of UF₆ was studied theoretically, and it was shown that an excess of 15 photons above the dissociation threshold was necessary to preserve the isotopic selectivity in 1 torr of UF₆ sample. This corresponds to the utilization of about 50 photons of 16 μm laser per UF₆ molecule dissociated. This knowledge would be useful in defining the optimum laser fluence requirement in IRMPD experiments on UF₆.

In the context of two-step photodissociation of UF₆ via an electronic excited state, photochemistry in its B–X band was studied using the 337.1 nm band of a pulsed N₂ laser. Decomposition of UF₆ yielded a mixture of solid products, identified as UF₅ and UF₄. The quantum yield ratio for these products was also determined⁶.

Sensitized multiphoton dissociation of UF₆ in SF₆–UF₆ mixtures was studied using a TEA CO₂ laser. The ν_3 mode of SF₆ absorbed the resonant CO₂-laser photons, and the vibrational energy thus gained was redistributed between different modes of SF₆. Since the ν_4 mode of SF₆ is close to the ν_3 mode of UF₆, rapid vibrational energy exchange took place between vibrationally-excited SF₆ and UF₆ molecules, and the latter got excited to the vibrational quasi-continuum by sequential absorption of CO₂-laser photons by SF₆ molecules and vibrational energy transfer. From the quasi-continuum, the UF₆ molecules, by further direct sequential absorption of CO₂-laser photons, got dissociated. Several experiments were carried out by irradiating pure SF₆, pure UF₆ and mixtures of SF₆ and UF₆ in different ratios with the P(20) line of the 10.6 μm band of the CO₂ laser, and the results were analysed⁷.

TEA CO₂ laser-induced photodissociation of UF₆ via interspecies V – V energy transfer from multiple-photon excited halomethanes was also studied. The dissociation of UF₆ sensitized by multiple-photon excitation of a series of halomethanes, CF₄, CF₃Cl and CF₂Cl₂, was investigated. The role of various experimental parameters like excitation frequency, fluence and pressure of the sensitizer/UF₆ on the dissociation yield was studied to evaluate the characteristics of the sensitizer/UF₆ system and the coupling of vibrational energy between the two mole-

cular systems. The efficiency of the energy transfer process was estimated on the basis of long range dipole-dipole interaction⁸.

Nozzle beam set-up and supercooling of SF₆

A conventional stainless steel continuous flow nozzle beam set-up was fabricated, the schematic of which is shown in Figure 9. A nozzle diameter (D) of 75 μm and stagnation pressures varying from 100 to 2000 torr were used in the experiments. SF₆ and SF₆-Ar mixtures prepared in an on-line mixing tube, were used in the supercooling experiments. The IR absorption spectrum of the supercooled SF₆ was recorded with a Laser Analytics LS3 diode spectrometer. The laser beam from the exit slit of the spectrometer was collimated and then focused with a KCl lens on the axis of the jet at a distance of 7.5 mm from the nozzle ($x/D = 100$). The transmitted laser beam was refocused with another KCl lens on a liquid nitrogen-cooled HgCdTe detector for intensity measurements. The output of the detector was processed by a lock-in amplifier and a desktop computer (HP 9825A), and plotted. Frequency calibration was done with NH₃ lines and a 3" thick germanium etalon.

The Q-branch region was surveyed. Features Q_A-Q_D seen in Figure 10 are the band heads formed by different groups of J -values arising out of octahedral splitting of the triply degenerate ν_3 band of SF₆ (ref. 9). The absorption in the Q-branch region was computed taking the molecular parameters and Clebsh-Gordon coefficients for SF₆ from the literature. The relative intensities of the band heads of the Q-branch of the ν_3 mode were used to determine its rotational temperature in the jet. The temperature so determined was verified by comparing the experimental and computed band contours (Figure 11). It may be seen from the figure that SF₆ was cooled to a rotational temperature of 9 K in our experiments¹⁰.

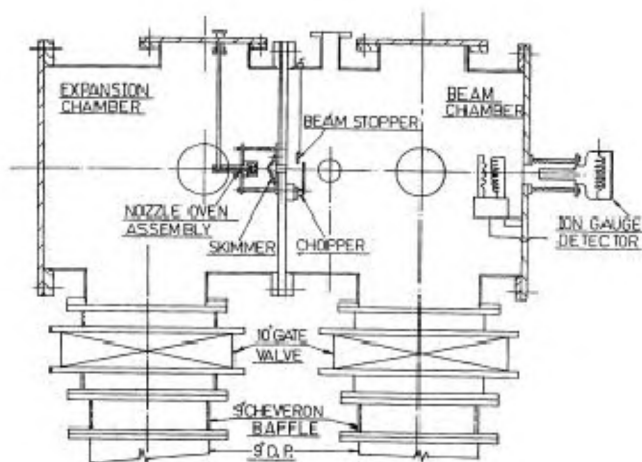


Figure 9. Nozzle beam set-up for studying supercooled vapour fabricated in our laboratory.

Theoretical formulations were developed to interpret time-of-flight data to characterize supersonic molecular beams in terms of translational temperature, speed ratio, flow velocity, characteristic velocity, terminal Mach number, collision effectiveness parameter and specific heat ratio^{11,12}. To obtain time-of-flight spectra, a collimated beam of pure SF₆ was produced by introducing a conical skimmer, 0.5 mm diameter, on the jet axis at a distance of 11 mm downstream from the nozzle exit. A pulse-type tuning fork, $f = 400$ Hz, generated molecular beam pulses which were detected at a distance of 41.5 cm away from the chopper by a fast ionization gauge detector, and averaged with a signal averager^{10,12}.

Flow velocity and characteristic velocity were obtained by fitting the observed signal profile, i.e. the TOF spectrum to a two-parameter number density function. From these parameters, speed ratio s , translation temperature T_{tr} and other beam parameters were determined. At 11 mm downstream from the nozzle exit, one could assume that $T_{\perp} = 0$ and $T_{\parallel} = T_{tr}$. The vibrational temperature, T_{vib} , was calculated from the experimentally determined T_{rot} and T_{tr} and the measured flow velocity u , using the energy balance equation. It was found that at higher stagnation pressures, T_{rot} and T_{tr} were close to each other, whereas the vibrational temperature lagged considerably behind them. For instance, for a stagnation pressure of 1000 torr, T_{tr} and T_{rot} are ≈ 30 K, whereas $T_{vib} \approx 265$ K. This can be understood since vibrational relaxation requires a large number of collisions, about 1000, while rotational relaxation requires only a few collisions^{10,12}.

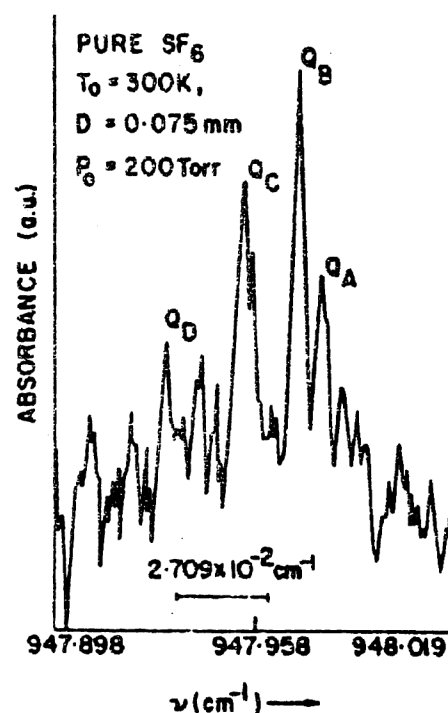


Figure 10. Diode laser absorption spectrum of the Q-branch of the ν_3 band of nozzle-cooled SF₆. $T_0 = 300$, $D = 75 \mu\text{m}$, $P_0 = 200$ torr. The spectrum was taken at the location $x/D = 100$.

The effective specific heat ratio, γ , and collision effectiveness parameter, ϵ , i.e. the change in random velocity per collision per molecule pertinent to jet expansion, were also determined as functions of the stagnation pressure. γ was determined by the experimentally measured T_{tr} (ref. 12). γ was high at moderate stagnation pressures, but decreased at higher stagnation pressures because of enhanced vibrational relaxation. These observations were explained in the light of the 'sudden freeze' and other models of vibrational relaxation^{11,12}. ϵ was found to be

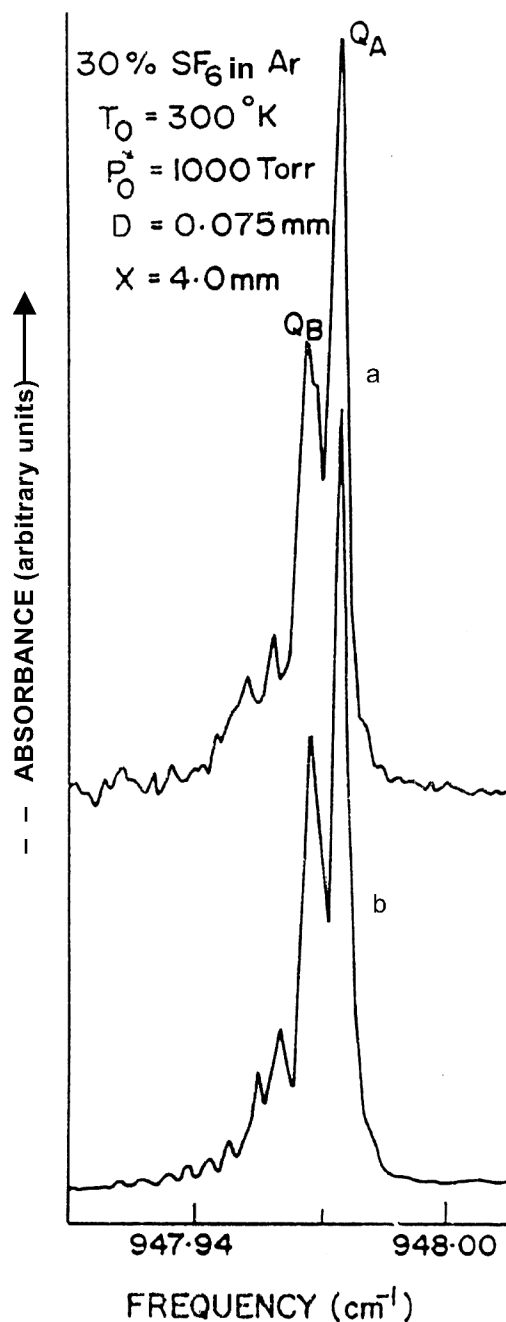


Figure 11. Experimental and computed absorption spectra of SF_6 . a, Nozzle-cooled absorption spectrum of 10% SF_6 seeded in Ar. b, Computed absorption spectrum of SF_6 at 9 K.

larger for argon than for helium under moderate stagnation pressures. Under such conditions, argon would give better translational cooling than helium¹⁰.

CF₄ laser

After extensive literature survey, it was decided that the CO_2 laser pumped CF_4 laser was among the best sources for generating step-tunable coherent radiation in the 15.3 to 16.3 μm region. This region overlaps with the ν_3 band of UF_6 , which has a well-resolved ^{235}U isotope shift in the nozzle-cooled spectrum. A schematic energy level diagram of CF_4 molecule is shown in Figure 12. The CO_2 laser pumps the $\nu_2 + \nu_4$ combination band of CF_4 molecule, and the lasing occurs on the hot band transition $\nu_2 + \nu_4 \rightarrow \nu_2$. The considerable fine structure of the CF_4 molecular band leads to step-tunable lasing on 80 lines, with a frequency tuning discreteness of 0.1 cm^{-1} .

Long CF_4 gas columns, up to 10 m at a typical pressure of ≈ 10 torr are necessary to ensure that a significant fraction of the CO_2 laser pump energy is deposited in the gas. The CF_4 laser output has a strong temperature dependence since the lower level of the lasing transition, being close to the ground state, has a significant thermal population. The best performance of CF_4 laser will, therefore, be obtained by keeping CF_4 at the lowest temperature with adequate vapour pressure. The CF_4 laser-absorption feature responsible for the 16 μm laser emission is resonant with the 9R(12) CO_2 laser line, and the desired pump frequency control is most readily achieved using a hybrid laser. The major requirements for a CF_4 laser are a tunable narrow bandwidth CO_2 pump laser and a long CF_4 cryogenic cell. The CF_4 laser was built by scientists of the then Laser Division at BARC. A brief description about the construction of the 16 μm CF_4 laser is given below. Details are available in Gupta *et al.*¹³.

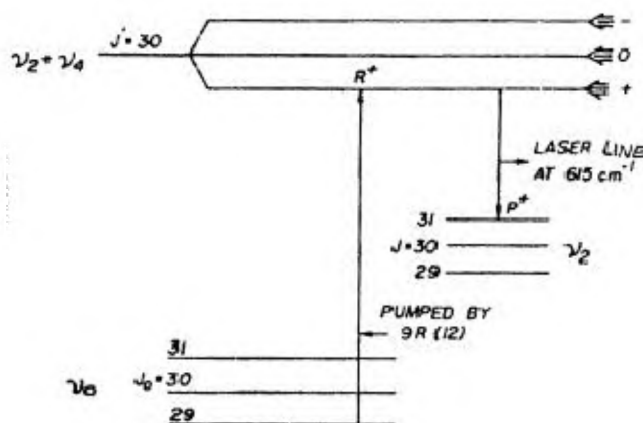


Figure 12. Energy-level diagram of CF_4 molecule. Three Coriolis sublevels of $J=30$ are denoted by $-$, 0 and $+$. CO_2 laser pumps the transition R^+ (29) populating the $+$ level of $J=30$. Stimulated emission occurs from this level to $J=31$ of ν_2 , producing the strong laser line P^+ (31) at 615 cm^{-1} .

CO₂ pump laser

A schematic diagram of the pump laser is shown in Figure 13. A line-tunable hybrid CO₂ laser oscillator provided 100 mJ output, on a single longitudinal mode near the centre of the 9R(12) line, to the TEA CO₂ laser amplifier, which amplified it to 1 J. The cryogenic cell (Figure 14) consisting of a 3 m long, 34 mm ID copper tube was placed in a stainless steel liquid nitrogen jacket, and heated by a three-segment teflon insulated heater. Temperatures of CF₄ down to 100 K could be obtained. Best CF₄ laser action was observed at CF₄ temperature of 115 K (vapour pressure 15 torr). The optical pumping arrangement used for the CF₄ laser is shown in Figure 15. The pump laser beam was gently focused with a long focal length lens in the centre of the cryogenic cell at a peak energy fluence of 1 J/cm². The 16 μ m output was separated from the pump CO₂ radiation by a combination of a LiF reststrahlen filter and a broadband dielectric filter. Under optimum conditions, 5 mJ of CF₄ laser output was obtained in the oscillator mode (Figure 15 a), 15 mJ in the Amplified Spontaneous Emission (ASE) mode arrangement (Figure 15 b) and 20 mJ in the ASE mode arrangement with mirror M_2 (Figure 15 c). In these experiments, 20 mJ output at 16 μ m was generated with about 200 mJ of CO₂ laser energy absorbed in CF₄ gas,

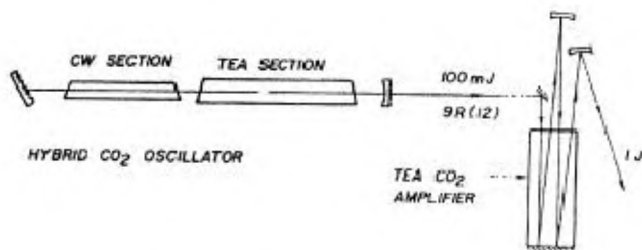


Figure 13. Schematic of CO₂ laser pump for CF₄ laser.

yielding an energy conversion efficiency of 10%, comparable to the best reported value.

Thus, the two basic infrastructural facilities for the enrichment of uranium by the UF₆-based approach – the set-up for supercooling molecular vapours to temperatures of a few Kelvin, and the line-tunable CF₄ laser were established and tested. Around 1985, the UF₆ approach was put on hold on the criterion that it was unlikely to compete with the atomic approach.

Atomic vapour laser isotope separation

With the few available lasers in the early 1980s, the best that we could hope to do was to carry out a proof of the principle experiment, i.e. to demonstrate that ²³⁵U ions are produced in excess of their abundance by isotopic selective excitation and ionization. To be able to do this experiment, adequate amounts of uranium vapour, \approx 0.1 torr, had to be produced, which necessitated heating uranium metal to \approx 2500 K. When the LIS programme was initiated, not much was known about the high-temperature properties of liquid uranium. Even the vapour pressure of liquid uranium above 2200 K was not known accurately. Compatibility of liquid uranium with materials like molybdenum, tantalum and tungsten, needed to handle it as containers, collimators, heat shields, etc. was not known. Therefore, studies on uranium at temperatures above 2000 K relevant to the atomic vapour laser isotope separation (AVLIS) process were taken up first.

Phase 1

High-temperature studies on uranium: It was decided to generate uranium vapour in a high vacuum chamber by heating a uranium compound/alloy in a suitable container by electron bombardment. We tried to identify a uranium

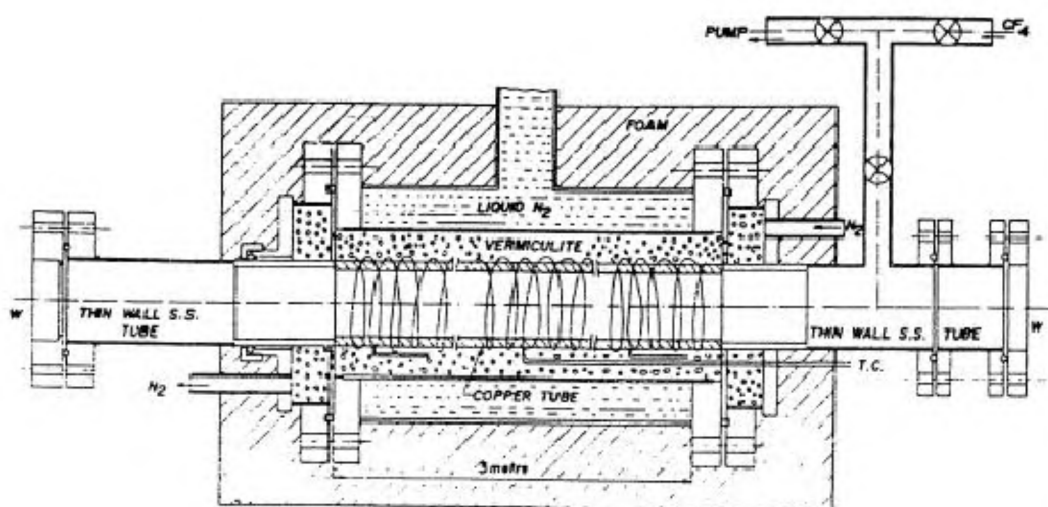


Figure 14. Schematic of cryogenic cell of CF₄ laser.

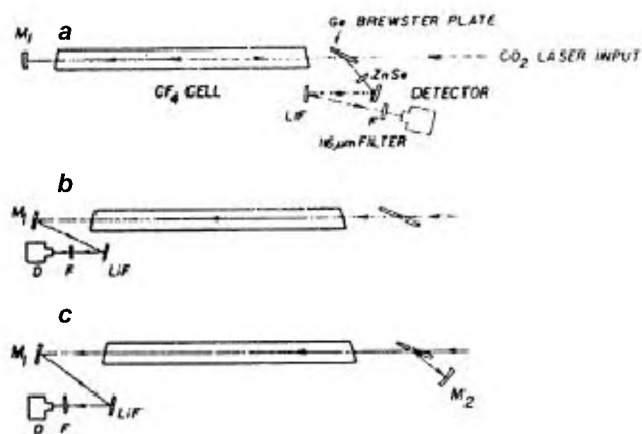


Figure 15. Pumping arrangement for CF_4 laser. *a*, Oscillator mode; *b*, ASE mode, and *c*, ASE mode with mirror M_2 .

compound that was less corrosive than the metal, but had uranium partial vapour pressure comparable to that of pure liquid uranium. In this context, the compounds uranium phosphide (UP) and uranium niobide (UNb) were prepared. Powder metallurgical tungsten containers of > 98% theoretical density, which were compatible to contain UP and UNb samples up to 2500 K and the alloy URe_2 up to 2800 K for extended periods, were developed¹⁴. Tantalum was found to be incompatible with all these materials above 2000 K. Ackerman and Rauh's spot method to locate the first formation of the liquid phase was combined with the determination of the solubility along the liquidus to obtain the high-temperature phase diagrams of the Re-U, Ta-U and W-U systems¹⁵. When UP and UNb were heated to high temperatures, the interfering role of the dissociation products, phosphorus and nitrogen, was found unacceptable. It was, therefore, decided to use URe_2 for experiments on isotope-selective ionization of uranium.

The next task was to extend the vapour pressure measurements on liquid uranium to 3000 K. The vapourization of uranium contained in single crystals of tantalum and tungsten was studied up to 3000 K in a Knudsen effusion assembly, shown schematically in Figure 16. The flux of U(g) vapour effusing through the Knudsen cell orifice was corrected for the solubility of Ta (or W) in liquid uranium, and its equilibrium vapour pressure was determined as:

$$\log(p_u^0/\text{atm}) = 6.295 - 2.642 \times 10^4/T.$$

We were thus able to extend the vapourization data of liquid uranium from 2200 to 3000 K. A reassessment of the available vapour pressure data using better thermal functions for U(g) and U(l) gave a value of 126.3 kcal/mol for the enthalpy of sublimation of uranium at 298.15 K (ref. 16).

Selective photoionization experiment

Evaporation system with electron bombardment heating

The assembly, named EMLIS 1 (experimental module-1 for LIS studies), consisting of a vacuum furnace based on electron bombardment heating was fabricated. URe_2 was contained in a 3 mm thick rectangular tungsten boat surrounded by a tungsten filament. The electrons emanating from the heated filament were accelerated towards the boat by a wattage-controlled 15 A, 15 kW power supply. The effusing uranium vapour was shaped into a beam by a tantalum collimator. A vacuum of 10^{-6} torr was maintained in the furnace. The uranium atomic beam passed through two grids for suppression of electrons and thermal ions in the beam. Uranium atom density of 6×10^9 atoms/cc was obtained in the interaction region, 5 cm above the boat, by heating the charge to 2400 K. The electron and photoion collector plates were maintained at a potential difference of 100 V. The current on the isotope collector, monitored using a charge-sensitive pre-amplifier, a passive band filter and a box-car averager, ensured 95% collection of the ions.

Laser system: This consisted of a Molectron UV-1000 N_2 laser with an average power of 250 mW at 20 Hz, and a dye laser of Hansch design, Molectron DL-100, with a band width of 0.03 cm^{-1} , pulse width of 8 ns, pulse energy of 125 mJ and 0.5 mm beam diameter. The dye laser pulses followed the N_2 laser pulses after 4 ns. A wave-

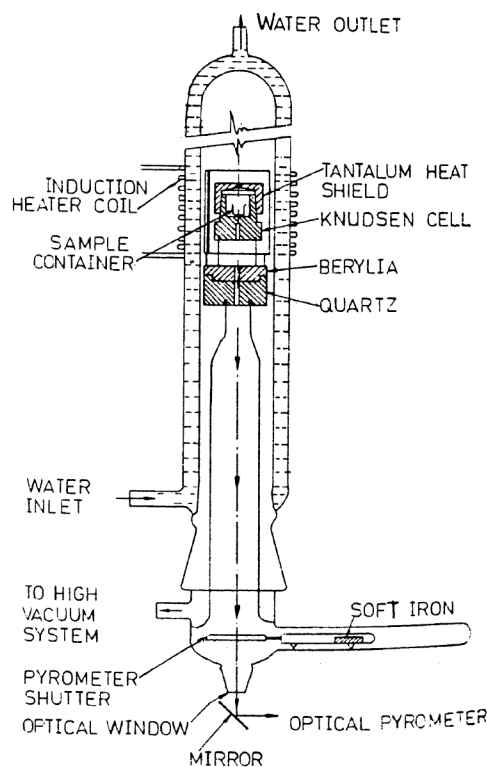


Figure 16. Schematic of the apparatus for high-temperature studies of uranium.

length control device using optogalvanic effect in a hollow cathode lamp was designed and developed to lock dye-laser wavelengths to atomic absorption lines for long durations¹⁷.

The experiment: The uranium line at 436.2 nm, with an isotope shift of 0.235 cm^{-1} and ^{235}U hfs width of 0.120 cm^{-1} , obtained using the Coumarin 120 dye with lasing peak at 438 nm, was chosen for selective excitation. The Coumarin dye was made in the Chemistry Division at BARC. The nitrogen laser band at 337.1 nm with a time delay of 10 ns, provided by a passive delay loop, was used as λ_2 . The divergences of the dye and the pump laser beams were matched to have maximum overlap in the interaction region by an appropriate lens system. The dye laser was first tuned close to the 436.2 nm line of ^{238}U with the help of a 1.5 m monochromator and onto the line using the optogalvanic signal from a uranium hollow cathode lamp, and the photoionization current was observed. The etalon in the dye laser with a $3'$ wedge in the plates had to be replaced with an etalon having no wedge, to avoid spurious etalon fringes. The flowing dye circulator had to be modified to improve the dye laser stability and decrease its line width to 0.03 cm^{-1} . The etalon scanning speed had to be reduced by a factor of ten to give adequate integration time for recording the weak OG signal of ^{235}U . With these various improvements, the dye laser was fine-tuned

to the ^{235}U line, using the known value of isotope shift in the line. The ^{235}U photoion current monitored showed a selectivity of 69%.

After establishing that uranium isotopes can be selectively ionized, we had to wait for some time to plan an isotope collection experiment. It was not possible to carry out the experiment unless a major improvement was made regarding uranium vapour generation. We decided to build an experimental chamber with provision for electron beam heating of a block of uranium, so that the liquid uranium formed could be contained in uranium solid, and the problem of containment of the highly reactive liquid was avoided. Also, uranium could be heated to higher temperatures to provide uranium atom densities a few times $10^{11}/\text{cc}$ in the laser–vapour interaction region.

Evaporation system with electron beam heating, EMLIS-2:

This consisted of a vacuum chamber placed between the poles of a large electromagnet. The chamber was made of a 300 mm diameter, 200 mm long, 6 mm thick stainless steel pipe mounted with its axis horizontal, as shown in Figure 17. The shell was provided with six ports used for viewing, evacuation, mounting the crucible, mounting the electron gun, coupling to the interaction region and a spare port. The shell was surrounded by a water jacket, and its two sides closed by water-cooled 295 mm diameter stainless steel flanges. A water-cooled stainless

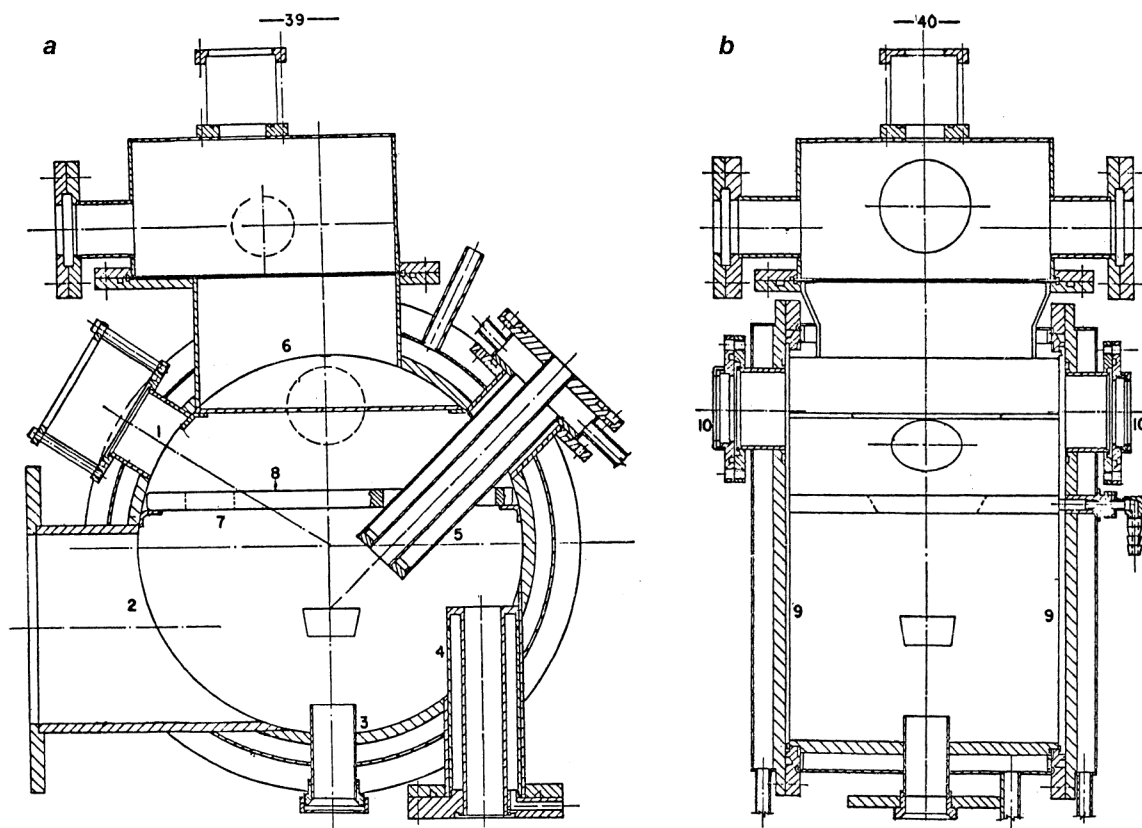


Figure 17. Experimental chamber EMLIS-2. *a*, Front view and *b*, Side view.

steel crucible, which could hold a 6 kg block of uranium, was mounted on port 3. In later experiments, a graphite insert was placed between the crucible and the uranium block so that the heat generated by the electron-beam evaporated uranium more effectively.

The chamber had three collimators, the first was 8.5 cm above the crucible, the distance being determined by the arc of the electron-beam trajectory. It was made up of 14 mm thick copper plate, with 6 mm diameter water-cooling channels drilled in it. The second collimator was 14 cm above the crucible, and the third 30 cm above it. The net vapour transmittance of the collimator system was about 1%.

The laser-atom interaction zone was in a rectangular cap welded over the cylindrical shell just above the third collimator. The laser beams passed through 5 cm diameter quartz windows. The isotope and tails collectors were located in the cap.

The electron gun was a Pierce-type gun used in the diode mode. A strip-type cathode was chosen for the gun because of its high thermal efficiency. The gun delivered a beam power of 10 kW in a spot of 4 mm diameter and could operate continuously for over 8 h. Since the gun produced a divergent electron beam at the exit of the anode, the beam had to be focused to get a good power density on the target. The focusing was done by a magnetic lens. To prevent the focused electron-beam from interacting with the externally applied magnetic field, all along its path, a double-walled water-cooled mild-steel tube was used to shield the beam. To hit the substrate vertically, at the exit of the tube, the electron-beam was bent by a magnetic field of ≈ 80 gauss provided by a discrete LC filter DC power supply. A 40 kV, 250 mA, 10 kW main electron-beam power supply, with several auxiliary power supplies and a number of safety interlocks to take care of all possible failure scenarios, provided power to the electron gun and the magnet. The electron gun and the electron-beam power supply were fabricated in the then Plasma Physics Division at BARC.

A C-core magnet was assembled to provide a magnetic field of up to 100 gauss to cover the lower part of the chamber. The magnetic field filtered the ions and electrons from the uranium vapour. The yoke of the magnet was a 8×5 cm section steel bar. The pole pieces were gradually tapered from 30 to 8 cm diameter (taper angle 30°), as shown in Figure 18. A 700-turn 10 ampere coil mounted at the centre of the yoke, and two 300-turn 10 ampere coils placed on the necks of the pole pieces gave a 100 gauss magnetic field over the required volume. A 10 ampere, 40 volt DC supply energized the magnet coils.

Uranium vapour generation experiments in EMLIS-2: The problems addressed here were the relationship between the electron-beam power incident on the target, the surface temperature of the target, evaporation rate, the

electron and ion contents in the uranium beam, etc. By adjusting the magnetic focus coil (FC) current, the electron-beam could be focused inside (post-focus), on (optimum focus) or above (pre-focus) the uranium block, resulting in different sizes of the electron-beam spot on the block. The beam size was minimum, 4 mm diameter, when the electron-beam was focused on the block.

The surface temperature T of the uranium block at the electron-beam spot was measured with a visual disappearing optical pyrometer. It was found that T was linear with the electron-beam power, P , up to the melting point of uranium, 1417 K. Later, the increase in T with P was slower, reaching the maximum temperature of 3000 K for an electron-beam power of ≈ 5.6 kW (28 kV and 200 mA). After T_{\max} , the temperature decreased with power¹⁸, as shown in Figure 19. A simple theoretical model was proposed to explain the nonlinearity of the temperature vs the electron-beam power behaviour, which fitted the observations well.

Only a fraction of the incident energy was used for the evaporation. The processes that take place in and around the point of impact of the electron-beam on the substrate are shown in Figure 20. A number of conditions prevailing in and around the evaporator affect the evaporation rate. It was measured to be 0.01 g/s in our chamber at the source temperature T_{\max} of 3000 K. From this, we could deduce the number density of uranium atoms in the interaction region to be $\approx 1.75 \times 10^{11}$. Use of a graphite insert raised the atom density to $2.50 \times 10^{11}/\text{cc}$, but lowered the useful run-time due to formation of UC.

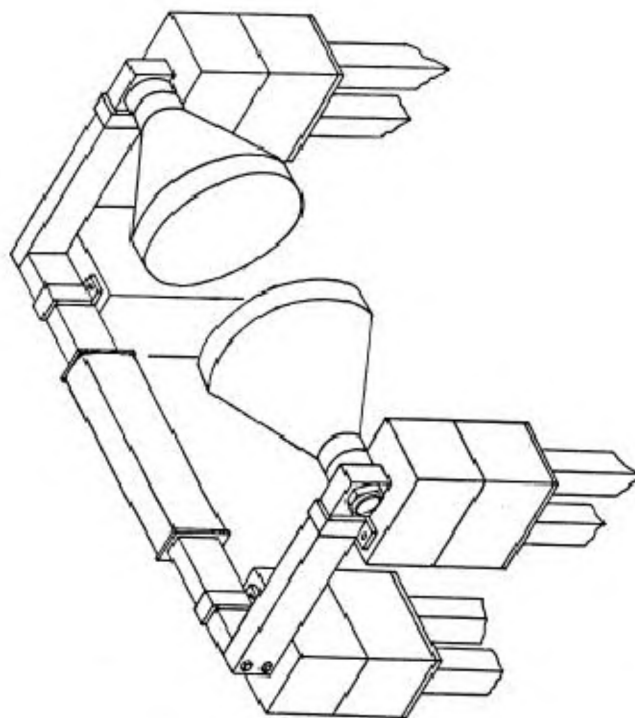


Figure 18. Schematic of the electromagnet.

The hot zone from which the vapour emanated was also a source of electrons and ions. These electrons are due to backscattering of the primary electrons, secondary electron emission, thermionic emission and photoelectrons produced by X-rays. At 3000 K, around 0.3% of uranium ions are produced due to Saha-ionization. Ions are also produced by collision of uranium atoms with electrons – primary and secondary.

Figure 21 shows the evaporation and ion current vs FC (lens) current curves¹⁹. It is seen that the maxima of the evaporation rate and the ion current correspond to slightly different FC currents. For a FC current of ≈ 500 mA, the evaporation rate P_1 was close to its maximum value, while the ion current was close to its minimum value, which is an ideal situation in our context.

From these experiments, optimum conditions for generation of uranium vapour, and suppression of ions and electrons were arrived at and used in later experiments.

Isotope collection experiment: The laser arrangement for these experiments was more or less the same as that used in the earlier experiments. The background ^{238}U photo-ion yield, with only the N_2 laser on, was measured to be 4×10^9 ions per pulse. When the dye laser tuned to the ^{238}U component of the 436.2 nm line and the N_2 laser with an appropriate time delay was used, the ion yield rose to 4×10^{10} . The dye laser was then tuned to the ^{235}U line, and the isotope collection experiment was carried out which gave an enrichment value several times above the uncertainty in mass spectroscopic analysis. In later experiments, using a highly shielded synchronized rotating isotope collector (Figure 22), a higher enrichment was achieved, which was about the best that could be achieved with the lasers available at that time.

Phase 2

It took some time before we could resume our next generation of enrichment experiments. We had to build high

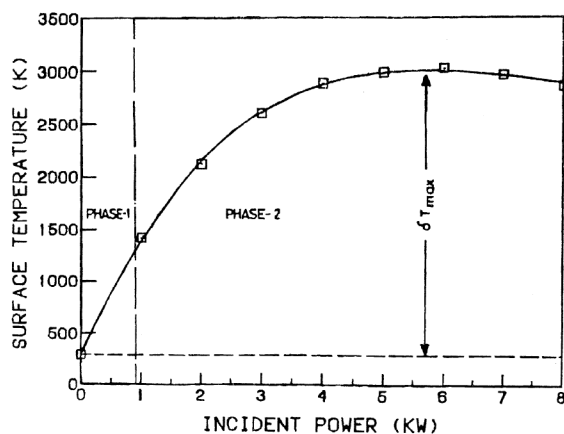


Figure 19. Surface temperature at the centre of uranium block as a function of the electron-beam power.

average power pump and dye lasers, and wavelength locking systems in adequate numbers. We also had to carry out a number of research investigations, experimental and theoretical, relevant to the AVLIS process.

We spent some effort in developing a high repetition rate, high average power N_2 laser. However, we wound up this effort when copper vapour laser (CVL) emerged as the best candidate for the high average power pump laser. CVL emits in the green ($\lambda_1 = 510.6$ nm, $\approx 70\%$ power) and the yellow ($\lambda_2 = 578.2$ nm, $\approx 30\%$ power) regions. It can be routinely operated at 6 kHz and can have a wall plug efficiency of $\approx 1\%$. Commercial CVLs of 25 W, CU25, were available from M/s Oxford Lasers, UK. We procured two of these and simultaneously started developing our own CVLs. We also started developing CVL pumped dye lasers.

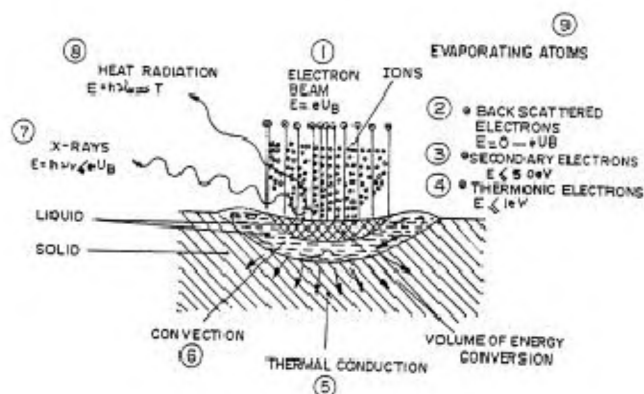


Figure 20. Processes taking place at the spot where the electron-beam is incident.

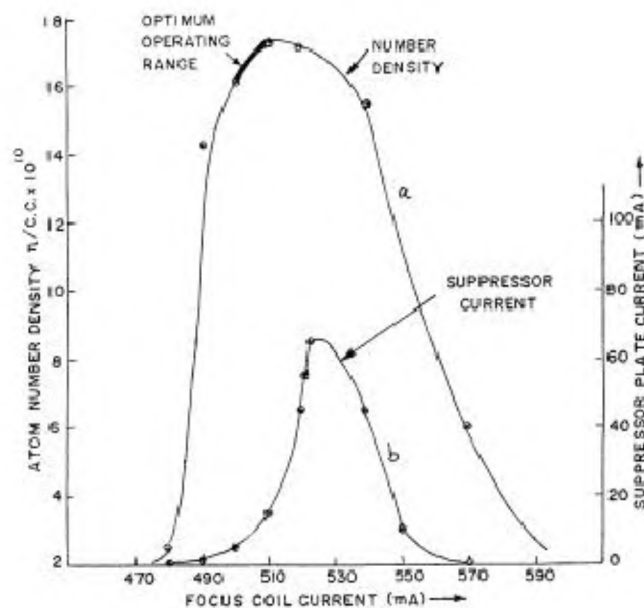


Figure 21. Curve (a), Atom number density vs focus coil current; Curve (b), Suppressor ion current vs focus coil current.

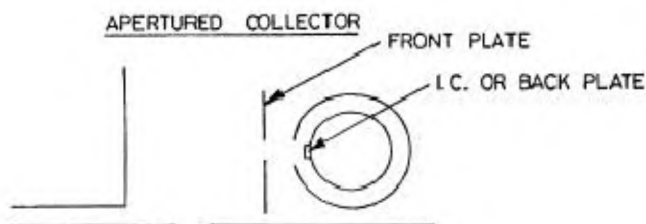


Figure 22. Schematic of the shielded rotating collector.

Since the shortest wavelength available from a CVL pumped dye laser was 565 nm ($\approx 17,700 \text{ cm}^{-1}$), the basic scheme to ionize an uranium atom with ionization potential of $49,958.4 \text{ cm}^{-1}$ has to involve three steps, i.e. it has to be a three wavelength ionization scheme requiring the use of three dye lasers.

AVLIS-related research and development activities

Development of CVL

The first CVL design was of a simple discharge heated type²⁰. The discharge tube consisted of a recrystallized alumina tube, 25 mm i.d. and 1.2 m long, placed concentrically in a pyrex glass vacuum envelope, 100 mm i.d. and 1.5 m long, with the help of end plugs, as shown in Figure 23. The plugs, made of mouldable alumina, were prefired at 1500 K to remove moisture. The annular space between the alumina and glass tubes was filled with alumina bulk fibre at a packing density of 250 g m^{-3} . The glass envelope was placed in a water-cooled stainless steel jacket, with a flange at one end mounted on insulating spacers to support the cathode. The water-cooled stainless steel flange had provision for mounting windows either at normal to the tube axis or at Brewster angle. A lining of perforated tantalum foil in the electrodes ensured that the discharge terminated with it.

To reduce the impurities during out-gassing of the thermal insulation, a buffer gas was used. The tube was loaded with 60 g of copper distributed at regular intervals along its length. The resonator cavity consisted of two plane mirrors, one with a reflectivity of 99.8% and the other of 8%, separated by 1.9 m. The CVL was a reson-

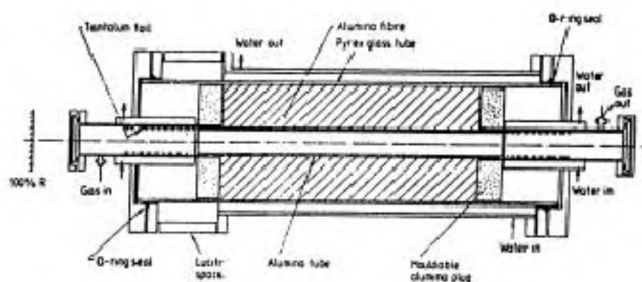


Figure 23. Schematic of the CVL discharge tube.

antly-charged thyatron-switched discharge device. An auxiliary AC discharge circuit was used to heat the tube initially. Later, the pulse modulator circuit was connected, thus saving the risk of damage to the thyatron at the time of start of the CVL.

The laser pulses at 510.6 and 578.2 nm were recorded after separation by a suitable filter. The emission at 578.2 nm was delayed by 20 ns with respect to that at 510.6 nm. This delay was important for the performance of CVL pumped dye lasers. An average power of 20 W at 6 kHz repetition rate was obtained for an input power of 4 kW, giving an efficiency of 0.5%.

Using an oscillator amplifier set-up, high peak power CVL pulses of short duration, $\approx 4 \text{ ns}$, were obtained. The output was nearly constant for a 40 ns delay variation between the oscillator and the amplifier²¹.

A simple and effective technique for significantly reducing the pulse width of a CVL without any reduction in its peak power was evolved, using intracavity spatial filtering. An average beam divergence of 0.45 mrad (\approx two times the diffraction limit) was achieved. Temporal pulse width of 3 ns fwhm was obtained²².

Using a positive branch self-filtering unstable resonator arrangement in the CVL, about 70% of the pulse energy was emitted in the diffraction angle. The resonator started influencing the mode behaviour of the output even during the first transit of the laser pulse. This would have a significant influence on the CVL Master Oscillator Power Amplifier (MOPA) characteristics²³.

Development of CVL pumped dye lasers

A low-power dye oscillator generated the desired wavelength, line width and beam quality. The oscillator output was boosted to high average power in one or more sequential dye-laser amplifiers operating at high efficiencies. Two approaches were possible – to develop single longitudinal mode dye oscillators with band widths of 60–100 MHz or multi longitudinal mode dye lasers with a band width 400 MHz–2 GHz.

We adopted the grazing-incidence-grating (GIG) resonator for the oscillator, shown schematically in Figure 24.

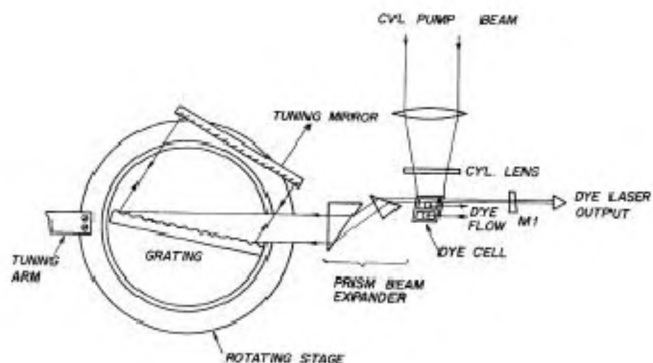


Figure 24. Schematic of the CVL dye laser oscillator.

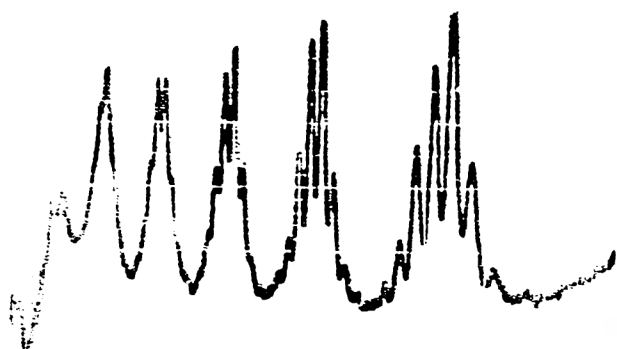


Figure 25. Storage oscilloscope trace of axial mode structure of CVL dye laser. Axial modes are separated by $\approx 0.02 \text{ cm}^{-1}$. The width of the axial mode, $\approx 0.01 \text{ cm}^{-1}$, is limited by instrument resolution.

The first-order diffraction beam from the GIG was reflected back into the resonator by a broad band high-reflecting tuning mirror. A double prism pre-expander was used to improve the laser efficiency. The narrow-band laser oscillator could be wavelength-scanned through the entire tuning range of the dye. The resonator was made short to minimize diffraction losses, and to achieve higher efficiency.

The dye laser oscillator was transversely pumped. A combination of spherical and cylindrical lenses was used to precisely position the CVL beam focus into the dye cell. The dye-flow system and the dye cell were specially designed to handle high repetition rate pump lasers. To avoid thermal lensing of the dye solution and consequent beam distortion, the dye was circulated rapidly to remove the volume heated by one pump pulse before the arrival of the next.

Efficient CVL-dye lasers in the wavelength range 570–680 nm use Rhodamine 6G, Rhodamine B, Kiton Red S and DCM dyes. Only the green line of CVL pumped the Rhodamine 6G dye, while the other dyes were pumped by both the green and yellow CVL lines. The axial mode structure of the dye-laser oscillator was recorded on a TV monitor and a storage oscilloscope. Eight axial modes, $\sim 300 \text{ MHz}$ wide, could be seen separated by $\sim 600 \text{ MHz}$ on the oscilloscope (Figure 25).

Wavelength locking device

A wavelength locking system was designed for the CVL dye laser (Figure 26). A part of the laser beam was taken through a temperature-controlled fixed air gap Fabry–Perot interferometer with fused silica spacers. Its reflecting surfaces were broadband coated for the visible region. The interferometer formed circular fringes, which were focused by a lens on a reflecting prism, on either side of which two diodes were arranged in such a way that both of them got illuminated equally, and their difference signal was zero. When the fringes expanded or contracted due to a change in the wavelength of the dye laser, the

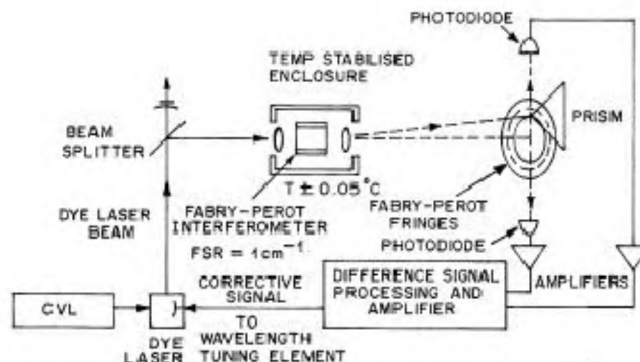


Figure 26. Schematic of the wavelength locking system for pulsed dye lasers.

photodiode difference signal went either positive or negative, and was used as the error signal to tune the laser back to the correct wavelength. The interferometer fringe locked to the position of the prism, followed it when given a translational motion. This slave motion of the fringe could be used for tuning the laser under lock over a range of 1 cm^{-1} (ref. 24).

Optics and optical coatings

The design of pump and dye lasers involved the use of several precision optical components and mounts. Precision optics and optical mounts were also required to transport CVL pump beams to dye lasers, dye laser beams to the interaction region, and combine three or four different wavelengths efficiently. Optical coatings play a crucial role in making high reflectors, partial reflectors, beam splitters and beam combiners to combine three or four laser λ s, having small wavelength differences, with minimum losses. Complex calculations are involved in designing the coatings – choice of the most appropriate dielectric materials, working out the optimum number of layers and thickness of each layer. Codes for achieving such complex designs were developed and tested.

We had set-up a machine shop and a precision optical workshop. Most of the optical components and mounts needed for our programme were made in these shops. There was also a state-of-the-art optical coating facility. All optical coatings required for our programme were computer-designed and produced in the facility.

Systematic studies on the dependence of optical constants on different evaporation parameters were made for a number of thin film materials. Using these data, high reflecting dielectric mirrors for the UV, visible and near-infrared regions were made²⁵. A thin film beam combiner was developed with an efficiency of better than 90%. The device, when operated at 45° angle of incidence, transmits in the UV and reflects in the visible region with minimum energy loss²⁶.

A new optimizing technique for designing multilayer optical thin film devices was developed, using the method of damped least squares with indirect reflection derivatives. Many constraints and boundary conditions compatible with the available experimental conditions were incorporated in the method, enabling it to give practically realizable designs²⁷.

A dual-technique laser calorimeter for measuring the absorption coefficient β and the extinction coefficient κ of dielectric thin films was developed. It measured the temperature rise and absorption of a sample simultaneously by a resistance thermometer and a temperature transducer²⁸. Several simple, non-destructive techniques for characterizing dielectric material in thin film form were developed. These include spectrophotometry, direct and indirect band gap analysis, interference enhanced Raman spectroscopy and appropriate computational procedures²⁹.

Atomic spectroscopy of uranium

Spectroscopic parameters of uranium: The spectroscopic parameters related to AVLIS are – energy level identifications, isotope shifts, hyperfine structures, excitation cross-sections from the ground and intermediate states, ionization and auto-ionization cross-sections from highly excited states, radiative lifetimes and branching ratios of excited states and cross-sections for excitation energy exchange, charge exchange and field-induced cross-sections. All available data on the spectroscopy and thermal properties of uranium atom relevant to AVLIS till 1988 were compiled in a report³⁰.

Uranium atom spectroscopy was studied extensively. A number of excellent reviews were available. However, most of the data were obtained from emission spectra of low excitation sources and from Fourier spectroscopy. There was paucity of data on intermediate and high-lying energy levels of uranium atom, like Rydberg and auto-

ionization levels, important in the second and final steps of the three-step ionization process. Also, data on isotope shifts in higher energy levels were scanty.

Extensive work on the spectroscopy of the uranium atom related to the AVLIS programme was carried out using different lasers. Several new energy levels of uranium atom were identified in the range 34,000–43,000 cm^{-1} , providing the upper levels of the second step wavelength λ_2 . Rydberg levels below the ionization limit (49,700–49,790 cm^{-1}) and autoionization levels above it (49,960–51,560 cm^{-1}), providing upper levels for the third step wavelength were also identified. Isotope shift measurements were made for a few high-lying uranium energy levels, i.e. for second step λ_s . These studies were made simultaneously by two groups – one using the Nd-YAG laser pumped dye laser and the N_2 laser pumped dye laser in the experimental chamber EMLIS-1, and the other using CVL pumped dye lasers and the uranium atom source located in a QMS system.

Uranium atom spectroscopy using Nd-YAG laser/ N_2 laser pumped dye laser

Several single-colour photoionization studies, using a dye laser pumped by the second harmonic of the Nd-YAG laser radiation were carried out. In single-colour experiments, there could be several routes leading to ionization – sequential two-photon excitation followed by ionizing third step, near resonant two-photon excitation followed by third-step ionization, etc. From one of these single-colour experiments, several odd parity levels of uranium were suggested in the region 34,000–43,000 cm^{-1} (see ref. 31). In another experiment shown schematically in Figure 27, λ was obtained by mixing the Nd-YAG laser pumped dye laser wavelengths, 559–569 nm, with the Nd-YAG laser fundamental at 1064 nm to obtain tunable wavelengths in the 365–372 nm region. From this

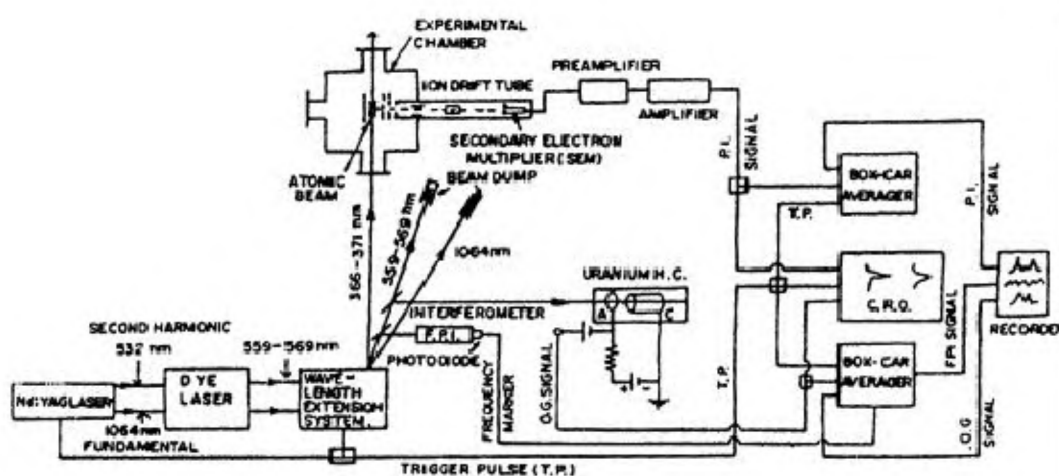


Figure 27. Schematic of the experimental set-up for single-colour photoionization studies of uranium in the EMLIS-1 chamber.

Uranium atom spectroscopy using CVL pumped dye lasers

lock-in amplifier combination, and fed to the first channel of a three-pen chart recorder. The OG signal from a uranium hollow cathode lamp generated by scanning the dye laser was fed to the second channel of the recorder. Interference signal produced by a small fraction of DL2 beam passing through an air-spaced FP etalon and detected by a photodiode went to the third channel of the recorder.

Using this set-up, a series of experiments was carried out locking λ_1 to five different uranium lines, one at a time, and recording two-colour ionization spectrum by scanning λ_2 . Several new odd parity levels of the uranium atom were identified in the region 34,290–35,120 cm^{-1} and their J values were assigned uniquely or with an uncertainty of one unit³⁷. To extend the range of search of odd parity levels, a second series of experiments was carried out, this time locking λ_1 to three uranium lines, one at a time, for all of which the metastable level at 3800 cm^{-1} , and not the ground state of uranium atom, was the lower level. By scanning λ_2 several new odd parity levels of uranium were identified in the 37,540–38,420 cm^{-1} region³⁸.

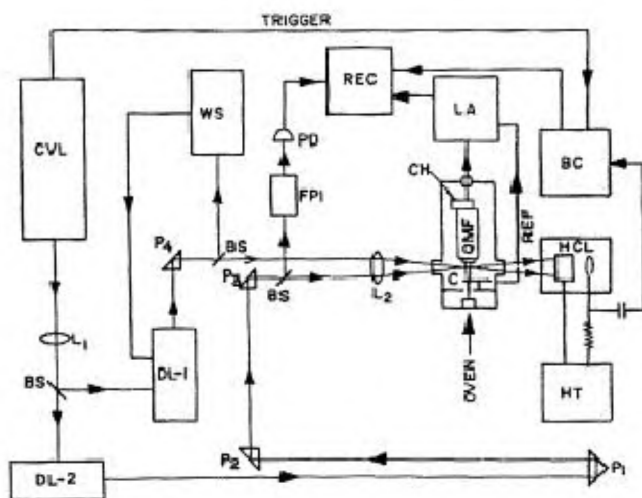
In another two-colour experiment, the energy level of uranium atom at $33,801\text{ cm}^{-1}$ was accessed by near resonant two-photon excitation. By scanning DL2 through $560\text{--}600\text{ nm}$, the region inside the ionization continuum $50,590\text{--}51,560\text{ cm}^{-1}$ was explored. As many as 230 even parity autoionization resonances were identified, some of these being very narrow (fwhm 0.1 cm^{-1}). Such resonances are used in actual enrichment experiments, since the ionization cross-section for λ_3 is high and one need not use high intensities to saturate the transition. In this experiment, a Rydberg series converging to the ionization limit of UII at 1749 cm^{-1} was identified³⁹.

From these experiments, some good combinations of the first and second-step wavelengths, λ_1 and λ_2 , both in terms of photoionization efficiency and isotope selectivity, were identified. In three-colour experiments to be described later, we shall discuss how λ_3 with the highest autoionization cross-section was identified.

A simple but elegant spectroscopic technique was developed for analysing single-colour resonant multiphoton ionization spectra. This technique, the pump-probe technique, used two narrow-band CVL pumped dye lasers to provide direct identification of the starting level of the multiphoton ionization pathway. The method can also be used to determine intermediate levels, which play an important role in the multiphoton ionization pathways⁴⁰.

Using two dye lasers, each pumped by a separate CVL, another technique was developed to measure isotope shifts in high-lying atomic levels of uranium, which was useful in choosing a good second-step wavelength⁴¹.

As a prelude to the enrichment experiments, the crucial three-colour experiments were carried out using CVL



CURRENT SCIENCE, VOL. 85, NO. 5, 10 SEPTEMBER 2003

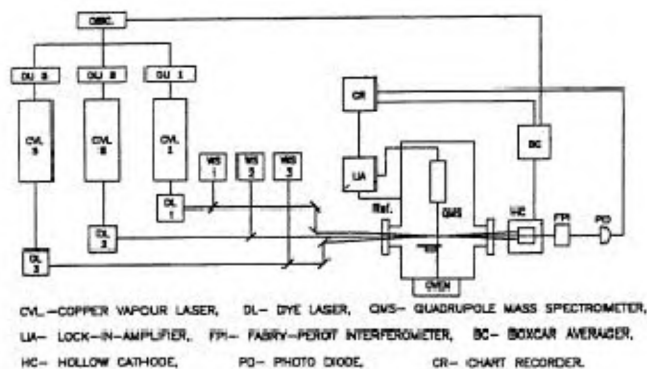


Figure 29. Schematic of the experimental set-up for three-colour photoionization of uranium in the quadrupole mass spectrometer system.

pumped dye lasers. A schematic of the experimental set-up is shown in Figure 29. Three dye lasers and two sets of wavelength locking devices were used. First, the QMS was set for ^{238}U ions. From the data already generated in our laboratory, a few of the best λ_1 , λ_2 sets for ^{238}U were chosen, and for each of these combinations, λ_3 , with an appropriate time delay, was scanned and the best λ_1 , λ_2 set giving the highest autoionization signals was selected. A typical autoionization spectrum of ^{238}U is shown in Figure 30. The QMS was then set for ^{235}U ions. Precise positions of λ_1 and λ_2 for ^{235}U , which are close to those for ^{238}U , were identified by iterative scanning of λ_1 and λ_2 , and the lasers were locked to those values. Then, λ_3 was scanned to yield three-colour autoionization resonances of the ^{235}U atom, which are the precise data required for enrichment experiments. Using these experiments, the most crucial task of identifying the precise λ_1 , λ_2 and λ_3 values for ^{235}U was accomplished. A mass scan of the QMS when λ_1 , λ_2 and λ_3 are tuned to ^{235}U lines, hardly shows any signal when the QMS passed through the ^{238}U position, indicating isotope-selective ionization of ^{235}U to be $\approx 100\%$.

Miscellaneous spectroscopic studies on U and UO

Some significant work was also carried out in the area of atomic transition probability measurements. The line absorption measurements were performed using a uranium hollow cathode discharge lamp as a light source as well as an absorption cell, and the relative transition probabilities of 20 uranium transitions involving the ground state and the metastable state at 620 cm^{-1} were measured^{42–44}.

Crossed laser beam – molecular beam configuration was employed to study photoionization of U and UO by the UV lines of an argon ion laser. The relative photoionization efficiencies of the two isotopic species of uranium were also investigated using a QMS⁴⁵. This was the first resonance ionization mass spectrometry publication from the laboratory.

Associative ionization of resonantly excited ($^5\text{L}_6-^7\text{M}_7$) atomic uranium with molecular oxygen was investigated

in a crossed beam configuration using a QMS. The laser-enhanced associative ionization cross-section, $5 \times 10^{-14}\text{ cm}^2$, for the formation of UO_2^+ ions was found to be three orders of magnitude higher compared to that of the ground state atom reaction⁴⁶.

Enrichment experiments

The hardware for the experiment consisted of three CVLs, three CVL-dye lasers, two wavelength-locking systems, QMS system, two time-delay units and beam-steering optics. The optical arrangement allowed small fractions of the three dye laser beams of λ_1 , λ_2 and λ_3 to pass through the cross-beam ionizer in the QMS, and the rest through the interaction region in EMLIS-2. The various pre-experiment steps included – start up and stabilization of the three CVLs, stabilization of the dye lasers, location and locking of appropriate dye laser λ s, generation and stabilization of the uranium vapour beams in the QMS and EMLIS-2, optical alignment of the λ_1 , λ_2 and λ_3 beams and the uranium vapour beams in the QMS and EMLIS-2, and setting approximate time delays between λ_2 and λ_1 , and λ_3 and λ_2 .

After all items were stabilized, the QMS was set for mass 238, λ_1 , λ_2 and λ_3 were set at the appropriate values determined in earlier experiments, and λ_1 and λ_2 were locked. The QMS was then set for mass 235, λ_1 , λ_2 and λ_3 were tuned to the ^{235}U atom, λ_1 and λ_2 were locked, and λ_3 was manually controlled. When all these parameters were set optimally, the shutter for uranium beam in EMLIS-2 was opened, and the enrichment experiment began. The ionization current in EMLIS-2 was constantly monitored, and any decrease was countered by slight adjustments of the electron-beam power, dye laser power, especially of DL3, position of λ_3 and the $\lambda_2 - \lambda_1$ and $\lambda_3 - \lambda_2$ time delays. The magnitude of the ionization current indicated how well the laser ionization process took place. The experiment was carried out for 30–45 min.

After the experiment was over, the tantalum isotope collector was taken out for extraction and quantitative estimation of the uranium collected on it. At this stage, a fairly good guess of what enrichment to expect was possible from the two data – ^{235}U ion current monitored during the experiment and the amount of uranium collected

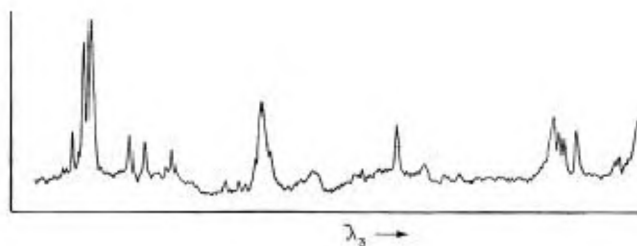


Figure 30. Autoionization resonances in the ^{238}U spectrum, recorded with λ_1 and λ_2 locked and λ_3 scanned.

on the isotope collector. The extracted uranium was sent for mass spectrometric analysis to the Radio Chemistry Division at BARC. The enrichment figure in the first experiment itself was high, a few times above our target figure.

The next experiment was carried out a week later, when all the units were made to work to their capacity. The CVL3 safety interlocks were countermanded for the duration of the experiment and run at the maximum power so as to get about 1 W output from DL3. The room housing CVL3 got heated-up in spite of air-conditioning. Every thing worked perfectly during the experiment, and the ionization current monitored in EMLIS-2 was found very high.

After the experiment the uranium was extracted from the collector plate and estimated. The enrichment value was several times our target figure of 2.5–3.0% ^{235}U .

Future possibilities

Though we had achieved high enrichment figures in our experiments described above, even higher enrichment and throughputs are possible. The ideal situation is when each uranium-235 atom that passes through the laser interaction region gets ionized and there is maximum utilization of laser photons. This is, to a good extent, possible. First, the intensity of DL3 (λ_3) can be increased to saturate the ionization step. Typically, DL1 and DL2 intensities oversaturate the first and second steps. Secondly, the effective repetition rate of the lasers could be increased three- or fourfold by temporal multiplexing of the lasers to process the entire height of the vapour column with cross-sectional area equal to that of the laser beams. Thirdly, the laser beams could be made to traverse the interaction region several times by multipassing the beams with appropriate optics. This, apart from processing larger volumes of the vapour, also allows optimum utilization of the laser photons. To further increase the throughput, the 25% population of uranium atoms available in the metastable state of uranium at 620 cm^{-1} , at the operating temperature of 2800 K, should be utilized. This will require the use of a fourth laser, at wavelength λ_{1A} , to pump the uranium atoms in the metastable state to the same first excited state to which λ_1 pumps uranium atoms from the ground state. Finally, the best possible combination of λ_1 , λ_{1A} , λ_2 and λ_3 has to be used. For instance, the λ_1 , λ_2 , λ_3 combination used in our final enrichment experiments is a good combination, but may not be the best possible. All these steps increase the number of ^{235}U ions produced for the same amount of ^{238}U scatter and effectively increase the enrichment value.

In the scenario of large throughputs, such high enrichment values will not be possible, and one has to make a compromise between the enrichment value and throughput requirements. For very high enrichment scenarios, a few stages of the AVLIS process will be necessary.

In the period between the successful completion of the enrichment experiments during mid-1988 and mid-1992, most of the efforts were aimed at building infrastructure for future large-scale experiments. These included designing and building larger LIS modules, higher powered electron-beam systems with linear focus, building more powerful CVL and dye laser systems, designing optics and optical coatings, which can withstand high laser powers. Besides, some experiments and theoretical computations, mostly the latter, were carried out in the areas of characterization of electron-beam-produced atomic vapour, atom-photon interaction, laser-beam propagation in atomic vapour and ion extraction. This is mentioned briefly below.

Design of large AVLIS systems

EMLIS-2B: This chamber was designed to have a uranium number density of $\approx 10^{12}\text{ cm}^{-3}$, five atomic streams providing $\approx 14\%$ vapour utilization and use of multiple pass optics. The main chamber, 0.612 m in diameter and 1.160 m long, consisted of three parts mounted horizontally. The central part, with its vacuum system, was mounted on a rigid stand. The two side chambers were hinged to the central chamber on either side. The side chambers housed all the optical components needed for multipassing the laser beams. A 20 kW electron-gun was used. The chamber was fabricated and preliminary experiments related to vapour generation, vapour characterization, etc. were carried out.

Development of a 20 kW electron gun

Based on the experience gained on Pierce-type 10 kW pencil beam electron gun, a 20 kW electron gun was designed. The design was essentially similar to that of the 10 kW gun, except for the use of a larger cathode and a bigger anode hole to enable extraction of a larger electron beam. Since, by now, the imported ceramic-to-metal seals were not available, the ceramic part was joined to the metal flange by a viton O-ring. Initially, this joint gave some outgassing problems, which were sorted out. A thyristor-regulated 20 kW power supply was procured from a local manufacturer. The 20 kW gun could be operated at the full power rating for several hours.

Lasers

High power CVL systems: The divergence of the output beam of a conventional stable resonator cavity CVL oscillator is high. It can be reduced using an unstable resonator cavity. Based on practical considerations, one has to decide on the power of the basic CVL oscillator, say 40 W. Its output, after spatial filtering, could be fed to a chain of CVL amplifiers to obtain the required higher

pump power. Since the number of elements in a chain is limited by super-radiant losses in a single pass through the amplifiers, there will be a limit to the power that could be obtained in a single chain. The desired CVL power for a high throughput experiment can be obtained by operating in parallel a number of identical CVL chains.

High power CVL-dye laser systems

The performance of the dye laser amplifier depends on many parameters, such as the energy and wavelength of the oscillator, CVL pump energy, delay between the oscillator and pump pulses, and dye concentration. For maximum efficiency, these have to be optimized. The amplifier is pumped transversely from both sides. Higher CVL pump power used for the amplifiers requires the dye-flow velocity in the active region of the amplifier cell to be high, which could be achieved by increasing the speed of dye circulation and decreasing the width of the dye flow in the region of the focal line of the pump laser. A direct vision prism and appropriate pinholes were used between the oscillator and the amplifier to prevent the oscillator amplified spontaneous emission from reaching the amplifier cell. The beam quality and spectral distribution of the oscillator could be retained in the amplifier by a careful adjustment of the amplifier parameters.

Conclusion

Separation of uranium isotopes was achieved using lasers. Three approaches to the problem were investigated – molecular approach using CO₂ laser and an appropriately tailored uranium-bearing molecule, another molecular approach using UF₆ and 16 micron laser and atomic approach using uranium vapour and tunable dye laser. Research infrastructure was established in all the three approaches. At a certain stage, a decision was taken to put on hold the two molecular approaches and concentrate on the atomic method, known as AVLIS.

In the AVLIS method, uranium vapour was produced around 2800 K and the uranium atoms ionized using three CVL pumped dye lasers. The isotopic selectivity achieved in the basic laser photoionization experiments was 100%. Uranium was enriched on a laboratory scale to several times our target figure of 2.5 to 3.0% ²³⁵U. The method developed is scalable, though some tough conventional and non-conventional engineering problems have to be solved. These include producing and handling kilograms of highly corrosive uranium vapour at 3000 K, photon engineering involved in the production and transport of kilowatts of pump laser power and hundreds of watts of dye laser power, fabricating and coating optical components which can withstand kilowatts of pump and dye laser powers.

1. Jensen, R., Marimuzzi, G. J., Robinson, C. P. and Rockwood, S. D., Prospects for uranium enrichment. *Laser Focus*, 1976, **12**, 5.
2. Job, V. A., Mittal, J. P., Ramakoteswara Rao, P. and Ganguly, A. K., Isotope separation by laser techniques. *Indian J. Phys.*, 1976, **50**, 302–316.
3. Rao, P. R. K., TEA–CO₂ laser initiated dissociation of SF₆. *J. Opt. Soc. Am.*, 1978, **68**, 687.
4. Cox, D. M., Hall, R. B., Horsley, J. A., Kramer, G. M., Rabinowitz, P. and Kalder, A., Isotopic selectivity of infrared laser-driven unimolecular dissociation of a volatile uranium compound. *Science*, 1979, **205**, 390–394.
5. Sarkar, S. K., Bajaj, P. N., Talukdar, R. K., Parthasarathy, V., Rama Rao, K. V. S., Mittal, J. P. and Chakraborti P. K., Thermal stability and IR-laser-driven selective photochemistry of a volatile uranyl compound at natural abundance. *Chem. Phys.*, 1987, **113**, 159–165.
6. Jyoti Subhiah, Sarkar, S. K., Rama Rao, K. V. S. and Mittal, J. P., Laser photochemistry of UF₆. *Indian J. Phys.*, 1980, **B54**, 121–131.
7. Karve, R. S., Sarkar, S. K., Rama Rao, K. V. S. and Mittal, J. P., Sensitized multiphoton dissociation of UF₆ in SF₆–UF₆ mixtures by a TEA CO₂ laser. *Chem. Lett.*, 1981, **78**, 273–276.
8. Karve, R. S., Sarkar, S. K., Rama Rao, K. V. S. and Mittal, J. P., TEA CO₂ laser induced photodissociation of UF₆, via interspecies V–V energy transfer from multiple photon excited halomethanes. *Appl. Phys.*, 1991, **B53**, 108–114.
9. Chakraborti, P. K., Kartha, V. B., Talukdar, R. K., Bajaj, P. N. and Joshi, A., Infrared diode laser diagnostic of supersonic free jets. *Chem. Phys. Letts.*, 1983, **101**, 397–400.
10. Chakraborti, P. K., Talukdar, R. K., Bajaj, P. N., Joshi, A. and Kartha, V. B., Relaxation in pure and seeded supersonic jets of SF₆. *Chem. Phys.*, 1985, **95**, 145–155.
11. Bajaj, P. N. and Chakraborti, P. K., Characterization of supersonic beams of polyatomic molecules. *Chem. Phys.*, 1986, **104**, 41–48.
12. Bajaj, P. N. and Chakraborti, P. K., Characterization of supersonic beams by time-of-flight technique. *Pramana – J. Phys.*, 1992, **38**, 397–409.
13. Gupta, P. K., Singhal, V. P., Shikarkhane, N. S., Sasikumar, S., Nundy, U. and Chatterjee, U. K., Design and operational characteristics of a 16 µm CF₄ laser. *Pramana – J. Phys.*, 1990, **34**, 249–257.
14. Das, D., Dharwadkar, S. R. and Chandrasekhariah, M. S., Containment of molten uranium alloys in powder metallurgical tungsten containers. *J. Nucl. Mat.*, 1981, **97**, 88–92.
15. Chandrasekhariah, M. S., Dharwadkar, S. R. and Das, D., High temperature phase diagrams of Re–U, Ta–U and W–U. *Z. Metallkde*, 1986, **77**, 509–512.
16. Das, D., Dharwadkar, S. R. and Chandrasekhariah, M. S., Thermodynamics of liquid uranium vaporization. *J. Nucl. Mat.*, 1985, **130**, 217–224.
17. Kapoor, R., Suri, B. M. and Saksena, G. D., Wavelength control for a pulsed dye laser using the optogalvanic effect. *J. Phys. E: Sci. Instrum.*, 1985, **18**, 930–932.
18. Bhatia, M. S., Joshi, A., Patel, K. and Chatterjee, U. K., Observation of non-linearity in e-beam evaporation from a water-cooled crucible. *J. Appl. Phys.*, 1989, **66**, 1159–1162.
19. Bhatia, M. S., Patel, K., Joshi, A. and Chatterjee, U. K., Control of ionization in e-beam evaporators via optimum choice of focus coil-current. *Rev. Sci. Instrum.*, 1989, **60**, 2794–2796.
20. Mittal, J. K., Bhadani, P. K., Singh, B., Abhinandan, L. and Bhatnagar, R. J., Design and performance of a 20 watt copper vapour laser. *J. Phys. E: Sci. Instrum.*, 1988, **21**, 435–438.
21. Singh, B., Nakhe, S. V., Dixit, S. K., Mittal, J. K. and Bhatnagar, R., Amplification of short (4 ns) copper vapour laser pulses. *Opt. Commun.*, 1991, **81**, 17–19.

22. Singh, B., Dixit, S. K., Mittal, J. K., Nakhe, S. V. and Bhatnagar, R., Effect of intracavity spatial filtering on the beam characteristics of a copper vapour laser. *Appl. Phys.*, 1991, **69**, 537–538.
23. Bhatnagar, R., Dixit, S. K., Mittal, J. K., Singh, B., Nakhe, S. V. and Sharangpani, K. K., A copper vapor laser with a positive branch self-filtering unstable resonator. *Opt. Commun.*, 1991, **82**, 557–562.
24. Manohar, K. G., Dasgupta, K., Suri, B. M. and Bhawalkar, D. D., Dye laser wavelength stabilization: An active control by interferometric fringe detection. *Rev. Sci. Instrum.*, 1987, **58**, 920–922.
25. Apparao, K. V. S., Dielectric mirrors for high power laser applications. *Bull. Mat. Sci.*, 1986, **8**, 339–342.
26. Apparao, K. V. S. and Sahoo, N. K., Design and development of a thin film dielectric beam combiner. *Bull. Mat. Sci.*, 1986, **8**, 343–346.
27. Apparao, K. V. S. R., A new optimization method of designing thin film devices. *Indian J. Pure Appl. Res.*, 1993, **31**, 457–463.
28. Sahoo, N. K. and Apparao, K. V. S. R., Laser calorimeter for UV absorption measurement of dielectric thin films. *Appl. Opt.*, 1992, **31**, 6111–6116.
29. Sahoo, N. K. and Apparao, K. V. S. R., Non-destructive characterization techniques for rapid optical and structural analysis of dielectric thin films. BARC/1993/E/014.
30. Ahmed, S. A., Pushpa, M. Rao and Jagtap, B. N., Energy levels, isotope shifts, hyperfine structures, life times, transitions probabilities and other spectroscopic parameters of neutral uranium atom update 1987, BARC-1433, 1988.
31. Mago, V. K., Lal, B., Ray, A. K., Rao, P. R. K. and Sharma, S. D., Single-colour photoionization studies of uranium I. *J. Phys. B: At. Mol. Phys.*, 1987, **20**, 6531–6539.
32. Mago, V. K., Ray, A. K., Lal, B. and Rao, P. R. K., Two-step single-color photoionization spectroscopy of atomic uranium. *Appl. Phys.*, 1993, **B56**, 39–42.
33. Ray, A. K., Lal, B., Mago, V. K. and Rao, P. R. K., Resonantly enhanced single-color multiphoton ionization of the uranium atom. *J. Opt. Soc. Am. B*, 1992, **9**, 1979–1987.
34. Ray, A. K., Mago, V. K., Lal, B. and Rao, P. R. K., New odd-parity Rydberg and autoionization levels in uranium I. *J. Opt. Soc. Am. B*, 1990, **7**, 145–150.
35. Mago, V. K., Lal, B., Ray, A. K., Kapoor, R., Sharma, S. D. and Rao, P. R. K., Two colour, three-step photoionization of uranium. *J. Phys. B: At. Mol. Phys.*, 1987, **20**, 6021–6030.
36. Mago, V. K., Ray, A. K., Lal, B. and Rao, P. R. K., Study of high-lying odd levels in UI by two-colour photoionization. *J. Phys. B: At. Mol. Opt. Phys.*, 1988, **21**, 955–961.
37. Suri, B. M., Dasgupta, K., Bajaj, P. N., Manohar, K. G., Talukdar, R., Chakraborti, P. K. and Rao, P. R. K., Observation of new high-lying odd levels of UI in a two-color multiphoton ionization spectrum. *J. Opt. Soc. Am. B*, 1987, **4**, 1835–1836.
38. Bajaj, P. N., Manohar, K. G., Suri, B. M., Dasgupta, K., Talukdar, R., Chakraborti, P. K. and Rao, P. R. K., Two colour multiphoton ionization spectroscopy of uranium from a metastable state. *Appl. Phys.*, 1988, **B47**, 55–59.
39. Manohar, K. G., Bajaj, P. N., Suri, B. M., Talukdar, R., Dasgupta, K., Chakraborti, P. K. and Rao, P. R. K., Observation of autoionization resonances in uranium by step-wise laser photoionization. *Appl. Phys.*, 1989, **B48**, 525–530.
40. Dasgupta, K., Manohar, K. G., Bajaj, P. N., Suri, B. M., Talukdar, R., Chakraborti, P. K. and Rao, P. R. K., Understanding single-color multiphoton ionization spectra by pump-probe technique. *J. Opt. Soc. Am. B*, 1988, **5**, 1257–1260.
41. Manohar, K. G., Bajaj, P. N., Vasdev, Chakraborti, P. K. and Rao, P. R. K., Isotope shift measurement of high-lying atomic levels by multi-step photoionization. *Pramana J. Phys.*, 1991, **37**, 539–544.
42. Kapoor, R. and Saksena, G. D., Simple technique to measure relative transition probabilities: Application to UI transitions. *Phys. Rev. Letts.*, 1988, **61**, 1481–1484.
43. Kapoor, R. and Saksena, G. D., Relative transition probabilities of neutral-uranium transitions. *J. Opt. Soc. B*, 1989, **6**, 1623–1626.
44. Kapoor, R. and Saksena, G. D., Transition probability of the 358.48 nm transition in neutral uranium from the line-absorption method. *Phys. Rev. A*, 1991, **44**, 784–787.
45. Talukdar, R., Tripathy, A., Bajaj, P. N., Chakraborty, P. K. and Saksena, G. D., Molecular beam study of photoionization of uranium and uranium oxide. *Opt. Commun.*, 1983, **45**, 179–182.
46. Bhowmick, G. K., Talukdar, R., Bajaj, P. N., Kartha, V. B. and Chakraborty, P. K., Associative ionization of laser excited uranium with molecular oxygen. *Chem. Phys. Letts.*, 1988, **144**, 407–411.

ACKNOWLEDGEMENTS. I thank Dr A. K. Ganguly, then Director Chemical Group and Dr R. Ramanna, then Director BARC, who had the vision to see the enormous possibilities of using lasers for isotope separation, and gave me full support to organize the research effort. Dr P. K. Iyengar helped in getting the EMLIS-2 chamber fabricated expeditiously in the Nuclear Physics Divisional Workshop, and made available an electron-beam unit from our Central Workshop. Bhusan Lal and P. K. Chakraborti, MDRS; D. D. Bhavalkar and U. K. Chatterjee, Laser Division; J. P. Mittal and K. V. S. Rama Rao, Chemistry Division and V. B. Kartha and G. D. Saksena, Spectroscopy Division coordinated the MDRS activity by direct participation as well as by guiding younger scientists. Chatterjee had also a significant role in the design of EMLIS-2 chamber. A. V. Thakur and his team were responsible for the development of electron-beam systems, R. Bhatnagar and his team for copper vapour lasers, Lalita Nair and her team for dye lasers. The activity was essentially a teamwork in which all scientists from MDRS and many scientists from several divisions at BARC worked in perfect synchronization. P. N. Bajaj, M. S. Bhatia, K. Dasgupta, A. Joshi, R. Kapoor, K. G. Manohar, A. K. Nayak, K. Patel, Sunder Das, B. M. Suri, R. Talukdar and Vas Dev participated in the final enrichment experiments.

Received 14 January 2003; revised 17 June 2003